





Multiple sclerosis lesions in motor tracts from brain to cervical cord: spatial distribution and correlation with disability

Anne Kerbrat,^{1,2}  Charley Gros,^{1,*} Atef Badji,^{1,3} Elise Bannier,^{4,5} Francesca Galassi,⁵ Benoit Combès,⁵  Raphaël Chouteau,² Pierre Labauge,⁶  Xavier Ayrignac,⁶ Clarisse Carra-Dalliere,⁶ Josefina Maranzano,^{7,8}  Tobias Granberg,⁹  Russell Ouellette,⁹ Leszek Stawiarz,⁹ Jan Hillert,⁹ Jason Talbott,¹⁰ Yasuhiko Tachibana,¹¹  Masaaki Hori,¹² Kouhei Kamiya,¹² Lydia Chougar,¹³ Jennifer Lefeuve,¹⁴  Daniel S. Reich,¹⁴ Govind Nair,¹⁴ Paola Valsasina,^{15,16}  Maria A. Rocca,¹⁵  Massimo Filippi,^{15,16} Renxin Chu,¹⁷ Rohit Bakshi,¹⁷  Virginie Callot,^{18,19} Jean Pelletier,^{19,20} Bertrand Audoin,^{19,20} Adil Maarouf,^{19,20} Nicolas Collongues,^{21,22,23} Jérôme De Seze,^{21,22,23} Gilles Edan² and Julien Cohen-Adad^{1,24}

*These authors contributed equally to this work.

Despite important efforts to solve the clinico-radiological paradox, correlation between lesion load and physical disability in patients with multiple sclerosis remains modest. One hypothesis could be that lesion location in corticospinal tracts plays a key role in explaining motor impairment. In this study, we describe the distribution of lesions along the corticospinal tracts from the cortex to the cervical spinal cord in patients with various disease phenotypes and disability status. We also assess the link between lesion load and location within corticospinal tracts, and disability at baseline and 2-year follow-up. We retrospectively included 290 patients (22 clinically isolated syndrome, 198 relapsing remitting, 39 secondary progressive, 31 primary progressive multiple sclerosis) from eight sites. Lesions were segmented on both brain (T₂-FLAIR or T₂-weighted) and cervical (axial T₂- or T₂*-weighted) MRI scans. Data were processed using an automated and publicly available pipeline. Brain, brainstem and spinal cord portions of the corticospinal tracts were identified using probabilistic atlases to measure the lesion volume fraction. Lesion frequency maps were produced for each phenotype and disability scores assessed with Expanded Disability Status Scale score and pyramidal functional system score. Results show that lesions were not homogeneously distributed along the corticospinal tracts, with the highest lesion frequency in the corona radiata and between C2 and C4 vertebral levels. The lesion volume fraction in the corticospinal tracts was higher in secondary and primary progressive patients (mean = 3.6 ± 2.7% and 2.9 ± 2.4%), compared to relapsing-remitting patients (1.6 ± 2.1%, both $P < 0.0001$). Voxel-wise analyses confirmed that lesion frequency was higher in progressive compared to relapsing-remitting patients, with significant bilateral clusters in the spinal cord corticospinal tracts ($P < 0.01$). The baseline Expanded Disability Status Scale score was associated with lesion volume fraction within the brain ($r = 0.31$, $P < 0.0001$), brainstem ($r = 0.45$, $P < 0.0001$) and spinal cord ($r = 0.57$, $P < 0.0001$) corticospinal tracts. The spinal cord corticospinal tracts lesion volume fraction remained the strongest factor in the multiple linear regression model, independently from cord atrophy. Baseline spinal cord corticospinal tracts lesion volume fraction was also associated with disability progression at 2-year follow-up ($P = 0.003$). Our results suggest a cumulative effect of lesions within the corticospinal tracts along the brain, brainstem and spinal cord portions to explain physical disability in multiple sclerosis patients, with a predominant impact of intramedullary lesions.

- 1 NeuroPoly Lab, Institute of Biomedical Engineering, Polytechnique Montreal, Montreal, Canada
- 2 CHU Rennes, Neurology department, Empenn U 1128 Inserm, CIC1414 Inserm, Rennes, France
- 3 Department of Neurosciences, Faculty of Medicine, Université de Montréal, QC, Canada
- 4 CHU Rennes, Radiology department, Rennes, France
- 5 Univ Rennes, Inria, CNRS, Inserm, IRISA UMR 6074, Empenn U1128, Rennes, France
- 6 MS Unit, Department of Neurology, CHU Montpellier, Montpellier, France
- 7 McConnell Brain Imaging Centre, Montreal Neurological Institute, Montreal, Canada
- 8 University of Quebec in Trois-Rivieres, Quebec, Canada
- 9 Department of Clinical Neuroscience, Karolinska Institutet, Stockholm, Sweden
- 10 Department of Radiology and Biomedical Imaging, Zuckerberg San Francisco General Hospital, University of California, San Francisco, CA, USA
- 11 National Institute of Radiological Sciences, QST, Chiba, Chiba, Japan
- 12 Toho University Omori Medical Center, Tokyo, Japan
- 13 Department of Neuroradiology, La Pitié Salpêtrière Hospital, Paris, France
- 14 National Institute of Neurological Disorders and Stroke, National Institutes of Health, Maryland, USA
- 15 Neuroimaging Research Unit, Institute of Experimental Neurology, Division of Neuroscience, and Neurology Unit, IRCCS San Raffaele Scientific Institute, Milan, Italy
- 16 Vita-Salute San Raffaele University, Milan, Italy
- 17 Brigham and Women's Hospital, Harvard Medical School, Boston, USA
- 18 AP-HM, Pôle d'imagerie médicale, Hôpital de la Timone, CEMEREM, Marseille, France
- 19 Aix-Marseille Univ, CNRS, CRMBM, Marseille, France
- 20 AP-HM, CHU Timone, Pôle de Neurosciences Cliniques, Department of Neurology, Marseille, France
- 21 Biopathologie de la Myéline, Neuroprotection et Stratégies Thérapeutiques, INSERM U1119, Fédération de Médecine Translationnelle de Strasbourg (FMTS), Université de Strasbourg, Bâtiment 3 de la Faculté de Médecine, 67 000 Strasbourg, France
- 22 Département de Neurologie, Centre Hospitalier Universitaire de Strasbourg, 67200 Strasbourg, France
- 23 Centre d'investigation Clinique, INSERM U1434, Centre Hospitalier Universitaire de Strasbourg, 67000 Strasbourg, France
- 24 Functional Neuroimaging Unit, CRIUGM, University of Montreal, Montreal, Canada

Correspondence to: Anne Kerbrat, MD, PhD
 CHU Hôpital Pontchaillou
 2 rue Henri Le Guilloux, 35033
 Rennes Cedex 9, France
 E-mail: Anne.kerbrat@chu-rennes.fr

Keywords: multiple sclerosis; corticospinal tract; MRI, disability

Abbreviations: CIS = clinically isolated syndrome; CST = corticospinal tract; EDSS = Expanded Disability Status Scale; PPMS = primary progressive multiple sclerosis; RRMS = relapsing-remitting multiple sclerosis; SPMS = secondary progressive multiple sclerosis; TWT = Timed 25-Foot Walk test; 9HPT = 9-Hole Peg Test

Introduction

The clinico-radiological paradox, i.e. the weak relationship between radiological findings and clinical consequences, is a still unsolved issue in multiple sclerosis (Barkhof 2002; Healy *et al.*, 2017). One hypothesis could be that lesion location, in addition to lesion load, plays a key role in explaining disability. In particular, progressive phenotypes of multiple sclerosis are most often characterized by a worsening pyramidal syndrome of lower and, to a lesser extent, upper limbs (Lublin *et al.*, 2014), suggesting a corticospinal tract (CST) involvement. Both clinical and MRI studies have provided evidence to support this hypothesis. First, patients with a solitary demyelinating lesion in the CST, mainly in the spinal cord lateral columns or anterior medulla, can develop progressive motor impairment, clinically very similar to progressive multiple sclerosis (Lattanzi *et al.*, 2014;

Keegan *et al.*, 2016). Similar observations were reported in progressive multiple sclerosis patients with few (i.e. two to five) lesions (Keegan *et al.*, 2018). Finally, in patients with more than five lesions but unilateral motor progression, the probability to detect lesions is higher in the CST corresponding to the motor deficit than on the contralateral side (Sechi *et al.*, 2019). However, these subgroups only represent a small portion of multiple sclerosis patients, who tend to have many more lesions and bilateral symptoms. In addition, these results were based on visual MRI assessment without quantitative measurement of motor tract damage.

To date, quantifying CST damage from the motor cortex to the spinal cord using MRI has not been fully explored in multiple sclerosis patients. In the brain portion of the CST, cross sectional studies revealed a moderate association between motor dysfunction and T₂-hyperintense (Riahi *et al.*, 1998; Daams *et al.*, 2015) and T₁-hypointense (Tovar-Moll *et al.*,

2015) lesion volumes. Metrics derived from diffusion tensor and magnetization transfer imaging in the brain CST also correlated with the pyramidal functional system score (Wilson *et al.*, 2003) and other specific clinical metrics reflecting motor function such as ankle and hip strength (Reich *et al.*, 2008; Fritz *et al.*, 2017) and the Timed 25-Foot Walk test (TWT) (Tovar-Moll *et al.*, 2015). In the spinal cord, magnetization transfer metrics in the lateral columns were correlated with ankle flexion strength (Zackowski *et al.*, 2009), and diffusion metrics were correlated with Expanded Disability Status Scale (EDSS), 9-Hole Peg Test (9HPT), and TWT scores (Naismith *et al.*, 2013). Lastly, in a recent study dedicated to lesion distribution in the cervical spinal cord, the lateral columns were more frequently affected by lesions in patients with progressive compared to relapsing phenotypes, and were significantly correlated with EDSS score (Eden *et al.*, 2019).

In the present study, we extend these investigations from the cortex to the cervical spinal cord, by specifically assessing CST lesion load in a large population of multiple sclerosis patients ($n = 290$) with various disease phenotypes and a wide range of disability status. After processing the data using an automated and publicly available pipeline, we (i) describe the distribution of multiple sclerosis lesions along the CST for each disease phenotype; (ii) assess the association between CST lesion load and location, and disability at baseline; and (iii) evaluate the association between CST lesion load and location, and disability progression after 2 years.

Materials and methods

Participants

Two hundred and ninety patients from eight centres were retrospectively included in the study. They were part of a previous study focused on cervical spinal cord lesion distribution (Eden *et al.*, 2019). Inclusion criteria were: (i) at least 18 years of age; (ii) a diagnosis of clinically isolated syndrome (CIS), relapsing-remitting multiple sclerosis (RRMS), secondary progressive multiple sclerosis (SPMS), or primary progressive multiple sclerosis (PPMS); the CIS patients had to fulfil the 2017 revisions of McDonald criteria for dissemination in space, and not for dissemination in time (Thompson *et al.*, 2018); (iii) available brain MRI images, including at least a 3D T₁-weighted and T₂-FLAIR or T₂-weighted brain scans; (iv) available spinal cord images covering the entire cervical cord, including at least an axial T₂-weighted or T₂*-weighted and sagittal T₂-weighted scans. Contrary to our previous work, all patients had both axial and sagittal scans with full coverage of the cervical cord in the two orientations, as lesions located in the lateral part of the spinal cord are often missed on sagittal scans; and (v) no diagnosis of degenerative cervical myelopathy or spinal cord trauma. The study was approved by each local institutional review board, and informed written consent was obtained from all participants.

Clinical assessment

At baseline, age, sex, disease duration and disease phenotype were collected. Overall neurological disability was assessed

using the EDSS ($n = 290$, 100%) (Kurtzke 1983). The degree of motor impairment was assessed using the pyramidal functional system score ($n = 206$, 71%). The TWT was used to assess lower limb function ($n = 222$, 77%) and the 9HPT upper limb function ($n = 118$, 41%) (Fischer *et al.*, 1999). At 2 years, the EDSS, and the pyramidal functional system score were available for 198 (68%) and 150 (52%) patients, respectively.

MRI data acquisition

Scans were acquired on 3 T MRI systems (Philips or Siemens), with varying protocols across sites as detailed in Supplementary Table 1. Brain sequences included: 3D T₂-FLAIR ($n = 243$, 84%), axial PD/T₂-weighted images ($n = 278$, 96%) used for brain lesion identification and 3D T₁-weighted images ($n = 290$, 100%) used for both brain CST identification via atlas registration and atrophy measurement. Spinal cord sequences included axial T₂*-weighted ($n = 198$, 68%) or T₂-weighted images ($n = 92$, 32%) from C1 to C7 vertebral levels, sagittal T₂-weighted ($n = 290$, 100%) and short TI inversion recovery (STIR) images ($n = 80$, 28%).

MRI data processing

Data were processed with an automated pipeline and publicly available (Fig. 1), using the *Spinal Cord Toolbox* v3.2.7 (De Leener *et al.*, 2017; <https://github.com/neuropoly/spinalcordtoolbox>), and *Anima Toolbox* (<https://github.com/Inria-Visages/Anima-Public>). Quality controls were performed after each processing step and systematically reviewed.

Brain MRI data processing

Focal T₂ lesion segmentation

Brain and brainstem T₂ hyperintense lesions were first automatically segmented using a method based on 3D convolutional networks on 3D T₂-FLAIR or axial T₂-weighted images (Valverde *et al.*, 2017) (Fig. 1, step 1). The network was fine-tuned for each centre multi-contrast data using a subset of 10 subjects manually segmented, and then used to infer on the remaining subjects. All binary lesion masks were then reviewed and manually corrected by two experienced raters (A.K., A.G.), blinded to clinical data.

Registration to ICBM template space

Intra-subject registration between the T₂-FLAIR (or T₂-weighted) and T₁-weighted data (Fig. 1, step 2a) was achieved using rigid transformations (Commowick *et al.*, 2012). Rigid, affine, and non-linear (Suarez *et al.*, 2012) transformations were successively computed (Fig. 1, step 2b) from the 3D T₁-weighted patient space and the ICBM template space (1 mm isotropic).

Lesion load quantification

The CST were identified after registering brain (Archer *et al.*, 2018) and brainstem (Tang *et al.*, 2018) probabilistic atlases to patient space (Fig. 1, step 3). For the brain, the CST descending from the primary motor cortex were considered (M1-CST). For each patient, total brain volume and the brain parenchymal fraction were computed from the 3D T₁-weighted images using an automatic segmentation method (Avants *et al.*, 2011). Absolute lesion volume and normalized lesion volume were

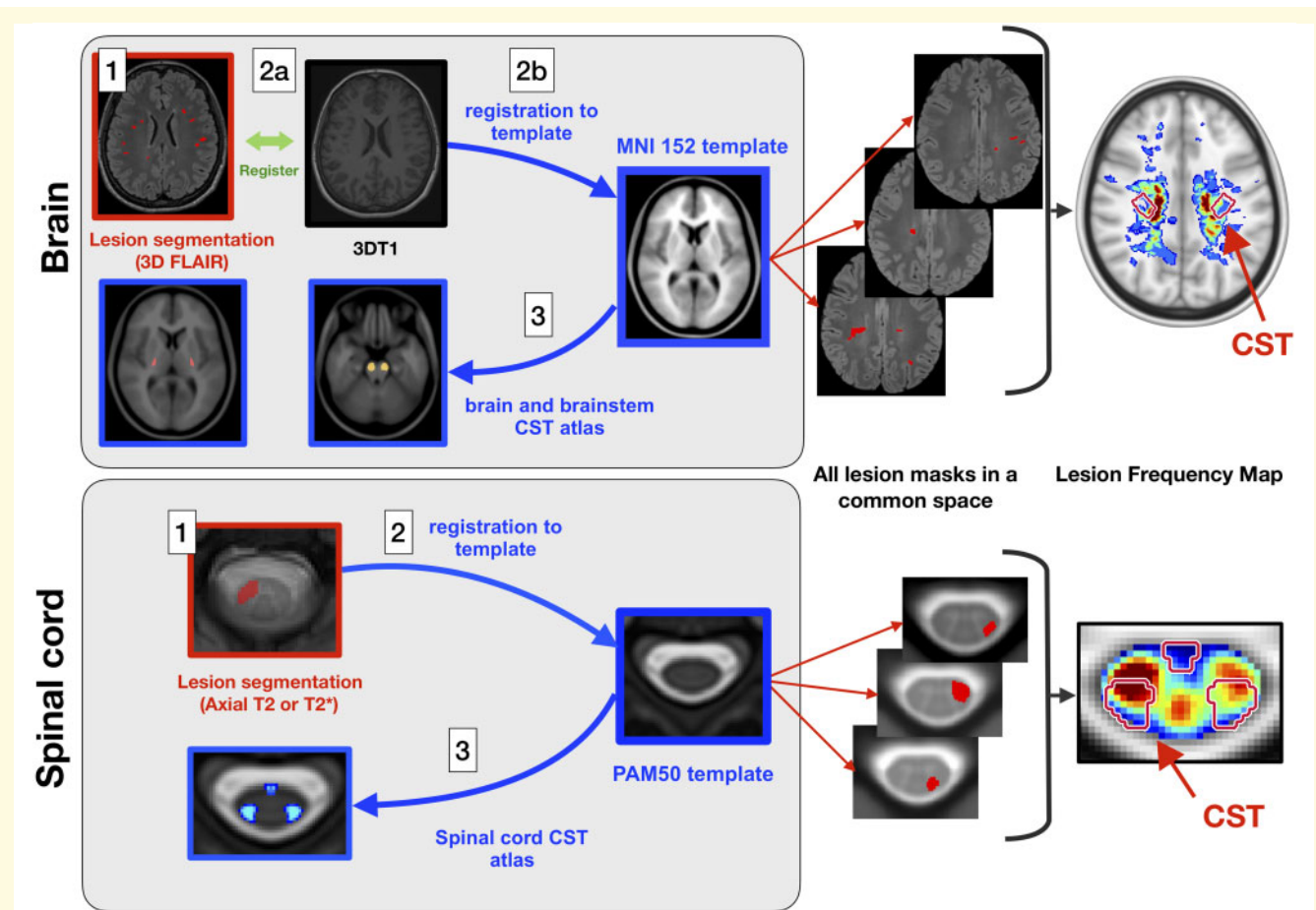


Figure 1 Processing pipeline. Brain data processing: (1) semi-automatic lesion segmentation on 3D T₂-FLAIR or axial T₂-weighted images (when 3D T₂-FLAIR was not available); (2a) intra-subject linear registration between T₂-FLAIR and T₁-weighted images; (2b) Affine and non-linear registration between T₁-weighted images and the T₁ ICBM 1 mm isotropic template space; and (3) quantification of lesion volume fraction based on brain and brainstem CST atlases. Spinal cord data processing: (1) manual lesion segmentation on axial T₂*-weighted images; (2) slice-wise non-linear registration to the PAM50 template; and (3) Quantification of lesion volume fraction based on a spinal cord CST atlas. To create the lesion frequency maps, brain and spinal cord lesion masks were averaged in the ICBM and PAM50 space, respectively.

computed in the native space of lesion masks. Absolute lesion volume refers to the total lesion volume within a region while normalized lesion volume refers to the total lesion volume within a region normalized to the volume of the region.

To validate the use of these atlases to identify the CST instead of patient tractography data, we compared the CST absolute lesion volume computed on a subset of 43 patients using both the atlas-based and tractography-based methods (Supplementary Fig. 1). In these patients, the CST descending from the primary motor cortex was identified using probabilistic tractography and a set of filtering regions of interest (Chouteau et al., 2019). The results of the two methods were highly correlated (Spearman correlation coefficient $r = 0.71$, $P < 0.0001$; Supplementary Fig. 2).

Spinal cord MRI data processing

Focal lesion segmentation

Nine raters manually segmented the axial T₂-weighted or T₂*-weighted images and the sagittal T₂-weighted and STIR images

used for the former study, and the inter-rater reliability was assessed in a subset of 10 patients (Eden et al., 2019) (Fig. 1, step 1). Only axial images with full coverage of the cervical cord were used in the present study and the axial lesion masks were systematically reviewed (A.K.), with complementary information from sagittal data. All raters were blinded to clinical data.

Registration to PAM50 template space

Multi-step non-linear transformations between each axial data-set and the PAM50 template (De Leener et al., 2018) were computed using registration parameters fine-tuned for this study (Fig. 1, step 2).

Lesion load quantification

The lateral and ventral CST were identified after warping the white matter spinal cord atlas (Lévy et al., 2015) to native space using inverse transformations. For each patient, the lesion count, absolute lesion volume, and normalized lesion volume were computed in the regions of interest (Fig. 1, step 3).

Cross-sectional area measurement

The spinal cord was automatically segmented on the axial T₂-weighted or T₂*-weighted images using a deep learning method (Gros *et al.*, 2019) implemented in the *Spinal Cord Toolbox*, and the segmentation was manually corrected when needed. The cross-sectional area was computed from the segmentation (number of pixels corrected for the angle between the slice and the cord centre line), and the values were averaged across slices between C2–C3 vertebral levels.

Generation of brain and cervical spinal cord lesion frequency maps

Brain and cervical spinal cord lesion frequency maps were produced in the corresponding template space by dividing the sum of lesion masks by the sum of brain or cord masks, on a voxelwise basis. Consequently, map intensities represent the frequency of a lesion occurring at each voxel across the whole dataset.

Statistical analysis

The characteristics of the study population were described for the whole cohort, for patients grouped by centre and by phenotype. Comparisons of the demographic data between disease phenotypes were conducted using the Mann-Whitney U-test. The independence between phenotypes repartition and centres were tested using Monte Carlo simulations. Unless otherwise specified, all tests were two-tailed and *P*-values were not adjusted for multiple comparisons.

Objective 1: To describe the spatial distribution of multiple sclerosis lesions along the CST

Lesion frequency maps were produced for the whole cohort and for patients grouped by phenotype. Difference of voxelwise lesion frequency between two patient groups were assessed using permutation testing (5000 permutations, using *fsl Randomise*) (Smith *et al.*, 2004) with unpaired *t*-test as test statistics, and including age, sex, disease duration and scanning site as nuisance variables. Significant clusters were identified with threshold-free cluster enhancement (Smith and Nichols, 2009) ($P < 0.05$, corrected for multiple comparisons across space). The anatomical location of the peak (i.e. maximum *t*-value) of each significant cluster was assessed using atlas-based analysis. The absolute and normalized lesion volume were also quantified on the whole-CST and on brain, brainstem and spinal cord-CST. Comparisons of these volumes within and between patients groups were performed using the *t*-test or the Mann-Whitney U-test.

Objective 2: Examining the link between CST lesion load in each region and disability at baseline

Lesion frequency maps were produced for patients categorized by EDSS score (low EDSS: 0–2.5; moderate EDSS: 3–5.5; severe EDSS: ≥ 6) and by pyramidal functional system score (low pyramidal functional system score: 0; moderate pyramidal functional system score: 1–2; severe pyramidal functional system score: ≥ 3). Multiple linear regression models were used to assess the voxelwise association between lesion location and EDSS or pyramidal functional system score, adjusted for age, sex, disease duration and scanning site (one-tailed for positive effect). The voxelwise analyses were repeated without adjustment for

scanning sites. Correlations between the normalized lesion volumes and clinical scores at baseline were measured using Spearman's correlation coefficient. Multiple linear regression models were then built to determine the link between normalized CST lesion volume (in brain, brainstem, and cervical spinal cord), and clinical scores (e.g. EDSS, pyramidal functional system score, TWT and 9HPT) at baseline, with adjustment for brain parenchymal fraction and cross sectional area and potential confounding factors (age, sex, disease duration, and scanning site). A backward stepwise linear regression was performed with a significance threshold of $P < 0.05$. We visually checked residuals and q-q plots, scale-location plots and residual versus leverage plots. The absence of strong collinearity between independent variables was checked using variance inflation factors. Subjects with missing relevant data were excluded. Similarly, other models were built to determine the link between whole brain, brainstem and spinal cord normalized lesion volume and clinical scores.

Objective 3: Determining the predictive value of CST lesions load in each region for disability progression at 2 years

A multivariable logistic regression was conducted to assess odd ratios of disability progression at 2 years of follow-up for the normalized lesion volume in the brain CST, brainstem CST, cervical spinal cord CST, brain parenchymal fraction, and spinal cord cross sectional area assessed at baseline. Analysis was adjusted for potential confounding factors (age, sex, disease duration, scanning site, EDSS at baseline). First, disability progression was defined as an increase in the EDSS of at least 1 point if the baseline EDSS was ≤ 5.5 , or 0.5 point if the baseline EDSS was > 5.5 . Second, disability progression was defined as an increase of at least 1 point of the pyramidal functional system score. These analyses were repeated in the subgroup of progressive multiple sclerosis patients. Results were expressed as odds ratios (OR) with 95% confidence intervals (CI) and the area under the curve of the global models were computed.

Data availability

Processing pipeline as well as the data supporting the findings of this study, including lesion frequency maps and detailed results from voxelwise analyses are available at: <https://osf.io/xqtnw/>.

Results

Demographic and clinical characteristics

The baseline group consisted of 22 patients with CIS, 198 with RRMS, 39 with SPMS, and 31 with PPMS. We observed a different repartition of disease phenotypes among centres ($P = 0.0005$) (Supplementary Table 2). The patient characteristics for the whole cohort and grouped by phenotype, are detailed in Table 1. At 2 years, the median EDSS remained stable at 2 (range: 0–8), but 48 of 198 patients (24%) had an increase in their EDSS compared with baseline. The median pyramidal functional system score was stable at 1 (range 0–5), but 29 of 150 patients (19%) had an

Table 1 Baseline demographic, clinical data, and global brain, brainstem, and spinal cord MRI characteristics

	All patients (n = 290)	CIS (n = 22)	RRMS (n = 198)	SPMS (n = 39)	PPMS (n = 31)
Baseline demographic and clinical data					
Sex F/M	185/105	15/7	128/70	24/15	18/13
Mean ± SD age, years	42.3 ± 12.2	42.7 ± 12.2	38.2 ± 9.8	51.9 ± 8.6	56.5 ± 12.6
Mean ± SD disease duration, years ^a	9.0 ± 9.8	4.6 ± 4.4	6.1 ± 7.1	22.0 ± 10.3	16.3 ± 10.9
Median EDSS (range)	2.0 (0.0–8.0)	1.0 (0.0–2.0)	1.5 (0.0–8.0)	6.0 (3.0–8.0)	6.0 (1.5–8.0)
Median pyramidal functional system score (range) ^a	1.0 (0.0–5.0)	0.0 (0.0–2.0)	0.0 (0.0–4.0)	3.0 (1.0–5.0)	3.0 (0.0–5.0)
Median TWT score (range) ^a	5.0 (2.8–112.0)	4.0 (3.6–5.2)	4.6 (2.8–34.0)	8.9 (4.5–40.0)	8.2 (4.0–112.0)
Median 9HPT (range) ^a	21.7 (16.1–81.6)	21.4 (18.7–28.3)	21.4 (16.1–65.0)	34.0 (23.4–81.6)	NA
Global brain, brainstem, and spinal cord MRI characteristics					
Brain					
Median absolute lesion volume (range), cm ³	3.5 (0–56.1)	0.7 (0.1–17.2)	3.1 (0–51.5)	7.9 (0.09–51.3)	5.9 (0.4–56.1)
Median brain parenchymal fraction (range)	0.79 (0.65–0.90)	0.79 (0.72–0.82)	0.80 (0.65–0.90)	0.76 (0.65–0.82)	0.77 (0.68–0.83)
Brainstem					
Median absolute lesion volume, cm ³ (range)	0.6 (0–14.4)	0.1 (0–5.6)	0.5 (0–8.6)	1.8 (0–10.4)	1.3 (0–14.4)
Cervical spinal cord					
Median absolute lesion volume cm ³ (range),	0.2 (0–2.1)	0.1 (0–0.4)	0.2 (0–2.1)	0.5 (0.1–2.1)	0.5 (0–1.6)
Median cord cross-sectional area across C2–C3 vertebral levels (range), mm ²	72.7 (44.2–124.3)	69.7 (61.8–82.6)	76.2 (52.5–124.3)	63.1 (44.2–84.5)	64.0 (52.6–80.8)

^aThe disease duration was available for 262 subjects, the pyramidal functional system score for 206 subjects, the TWT score for 222 subjects and the 9HPT for 118 subjects. NA = not available for PPMS patients.

increase in their pyramidal functional system score compared with baseline.

Description of multiple sclerosis lesion distribution along the CST for the whole cohort

Lesion frequency maps

All patients except three CIS and four RRMS patients had at least one lesion affecting their CST. Lesions were not homogeneously distributed along the CST (Fig. 2A). Overall, lesions were more frequent in the corona radiata for the brain and from C2 to C4 for the spinal cord (voxel frequencies > 10%, Fig. 2A, left column), whereas lesions were less frequent in the brainstem. In the axial plane, high lesion frequency was mainly found in the medial part of the CST in the corona radiata, whereas the entire spinal CST were highly affected between C2 to C4.

Lesion volume in the brain, brainstem, and spinal cord CST

Across all patients, the median percentage of lesion volume within the whole CST was 1.2% [interquartile range (IQR): 0.4–2.6%]. The normalized lesion volume was higher in the spinal CST (median: 3.3%, IQR: 0.9–8.3%) compared to the brain CST (0.6%, 0–2.0%, $P < 0.0001$) and the brainstem CST (0%, 0–0.5%, $P < 0.0001$). In the corona radiata, the normalized lesion volume was higher in the medial part of the CST compared to the lateral part (1.1%, 0–5.6% versus 0.29%, 0–2.15%, $P = 0.0001$). The correlations between the CST normalized lesion volume in the spinal cord portion versus the brain or brainstem portion were $r = 0.22$

($P < 0.001$) and $r = 0.32$ ($P < 0.0001$), respectively. The correlation between CST lesion volume in the brain portion versus the brainstem portion was $r = 0.37$ ($P < 0.0001$).

Description of multiple sclerosis lesions distribution along the CST according to disease phenotype

Lesion frequency maps

CST lesions were more frequent in progressive patients (Fig. 2A, two right columns) compared to RRMS (third column) and CIS patients (second column). However, locations of higher lesion frequencies were similar across phenotypes (Fig. 2B). Lesions were more frequent in the spinal cord portion of the CST in progressive versus relapsing patients. The lesion frequency maps were similar between SPMS and PPMS patients.

Voxelwise comparison between phenotypes

Voxelwise comparisons confirmed that lesion frequency was higher in SPMS patients compared to RRMS patients. Significant clusters were found in the spinal cord in the left and right CST (Fig. 3), with a peak in the right lateral CST at vertebral level C3–C4 (peak t -value: 5.8, $P = 0.002$). Significant clusters were also found in the brain, mainly in the frontal lobes, outside the CST (peak t -value in the right frontal lobe: 5.6, $P = 0.02$). Similarly, lesion frequency was higher in PPMS patients compared to RRMS patients with significant clusters in the spinal cord, both inside and outside the CST (Fig. 3), with peaks at C6 in the posterior spinal cord (peak t -value: 7.5, $P = 0.0006$) and in the right lateral CST (peak t -value = 7.0, $P = 0.0008$). In the brain, a small

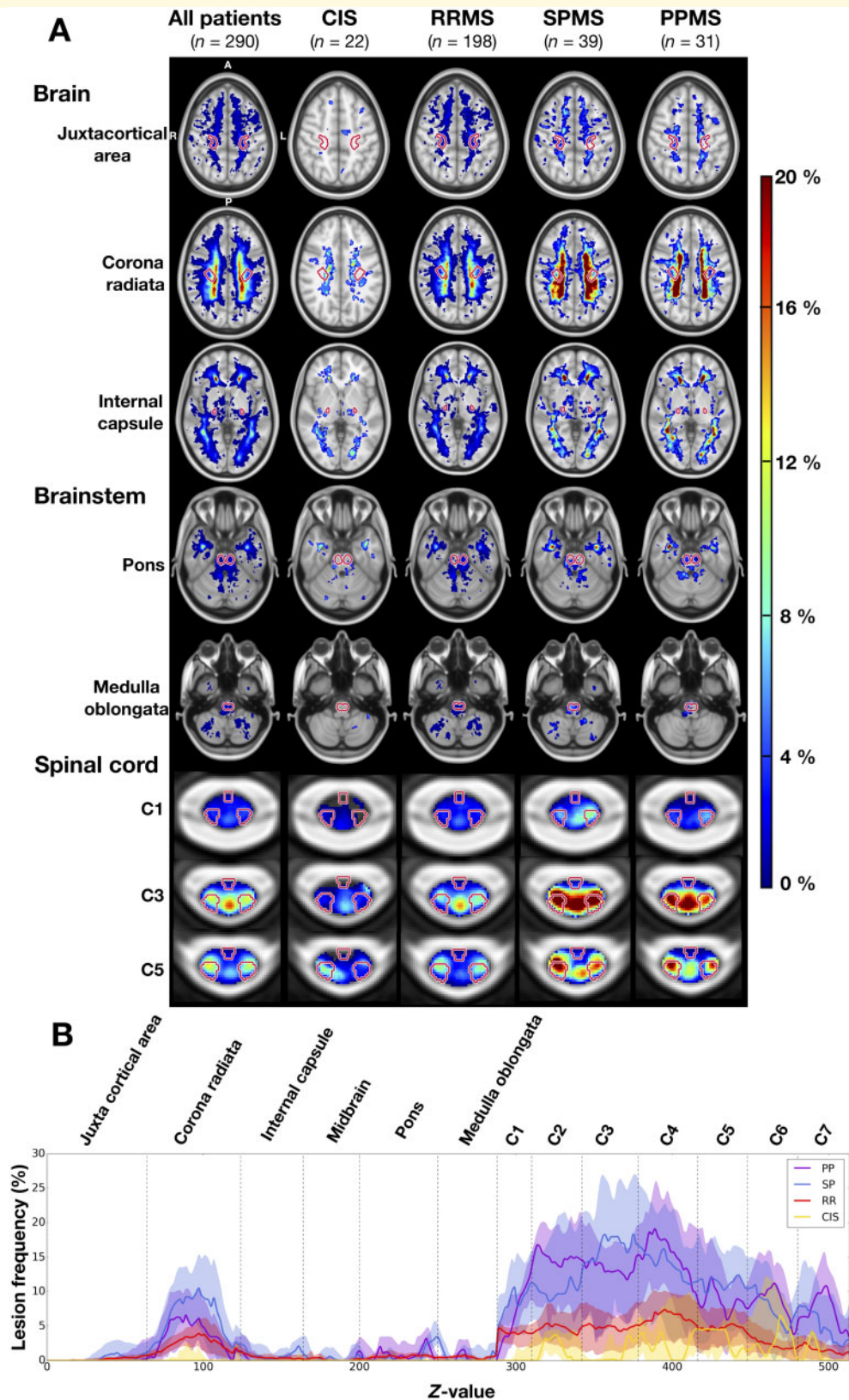


Figure 2 Lesion frequency in the brain, brainstem and cervical spinal cord. (A) Lesion frequency maps for the whole cohort and for each disease phenotype. The CST are indicated in red contour. (B) Lesion frequency along the CST for each phenotype subcohort. For each axial slice (1-mm slice thickness), the CST lesion frequency median and interquartile range are represented by a solid line and shaded region, respectively. The CST segments are demarcated by dashed vertical lines. When interpreting this graph, it is important to keep in mind that the lesion frequencies are normalized by the CST volume.

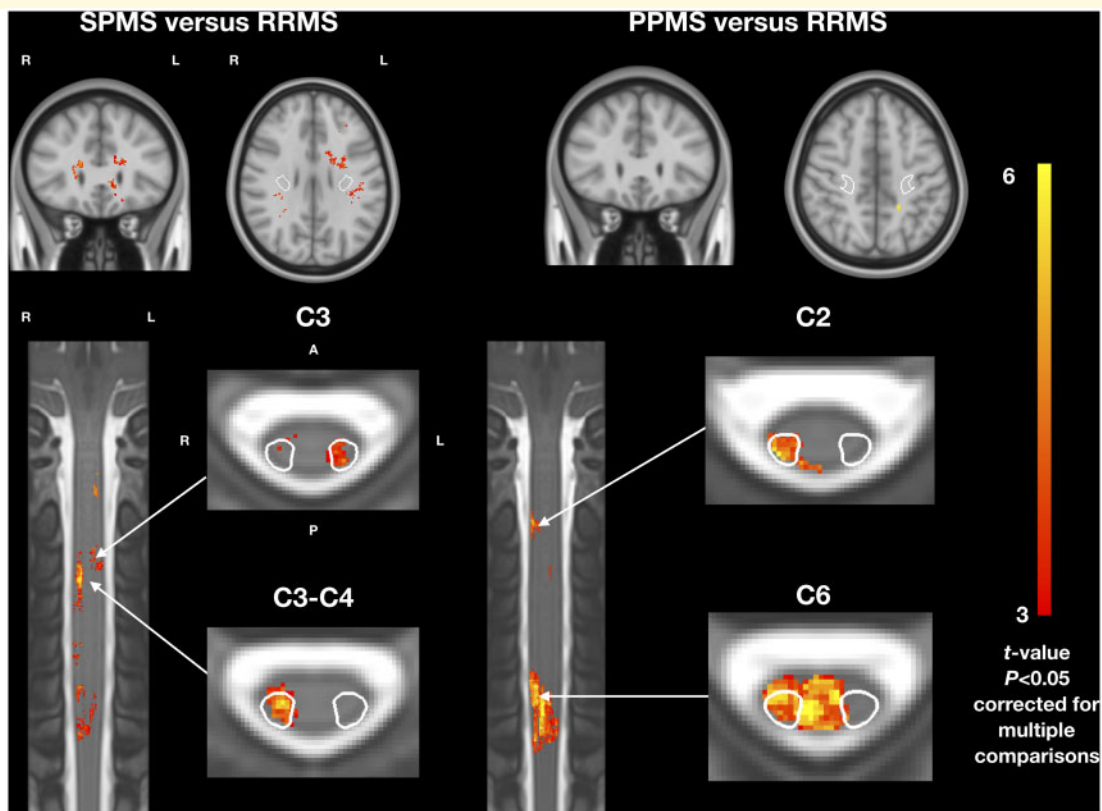


Figure 3 T_2 lesion frequency voxelwise comparison between phenotypes. (A) Patients with SPMS versus RRMS. (B) Patients with PPMS versus RRMS. Coronal and axial views. Only t -values of voxels from significant clusters are shown ($P < 0.05$, family-wise error corrected for multiple comparisons). All analyses were adjusted for sex, age, disease duration and scanning sites. A = anterior; P = posterior; L = left; R = right. The CST is indicated in white contour in axial views.

significant cluster was found in the left parietal lobe (peak t -value = 6.1, $P = 0.04$). We did not observe evidence for differences between SPMS and PPMS patients.

Absolute and normalized lesion volume in the brain, brainstem, and spinal cord CST

The absolute and normalized lesion volumes in the CST for each phenotype are detailed in Fig. 4 (see also Supplementary Table 3 for values). In the whole CST, the absolute lesion volume was lower in CIS patients compared to RRMS ($P < 0.05$), SPMS and PPMS patients ($P < 0.0001$) and lower in RRMS patients compared to SPMS and PPMS patients ($P < 0.0001$). No significant difference was found between SPMS and PPMS ($P = 0.4$). The absolute lesion volume in the brain CST was lower in CIS patients compared to RRMS, SPMS and PPMS patients ($P < 0.01$) and lower in RRMS patients compared to SPMS patients ($P = 0.03$). No significant difference was found between RRMS and PPMS ($P = 0.4$) and between SPMS and PPMS ($P = 0.4$). Both the brainstem and spinal cord CST had a lower absolute lesion volume in CIS patients compared to SPMS and PPMS ($P < 0.0001$) and in RRMS compared to SPMS and PPMS ($P < 0.0001$, except for RRMS versus PPMS in the brainstem: $P < 0.001$). No significant difference was found

between CIS and RRMS patients and between SPMS and PPMS patients. Overall, the results were the same when using the normalized lesion volumes in the CST.

CST lesion load and location, and disability at baseline

Lesion frequency maps

An increased lesion frequency was observed for patients with higher EDSS score (Supplementary Fig. 3). In particular, patients with severe pyramidal functional system score (3 or more) had higher lesion frequencies in their CST compared to patients with low or medium pyramidal functional system score (Fig. 5A and B).

Voxelwise associations with disability

Voxelwise analyses showed that EDSS score (Fig. 6A), adjusted for age, sex, disease duration and scanning sites, was associated with lesion frequency in both the brain and the spinal cord. The strongest correlations assessed by the t -value were found in the right lateral CST at C4 for the spinal cord (peak t -value: 7.6, $P = 0.0002$) and in the left corona radiata, outside the CST (in the parietal lobe) for the brain (peak t -value = 6.7, $P = 0.0002$). The pyramidal

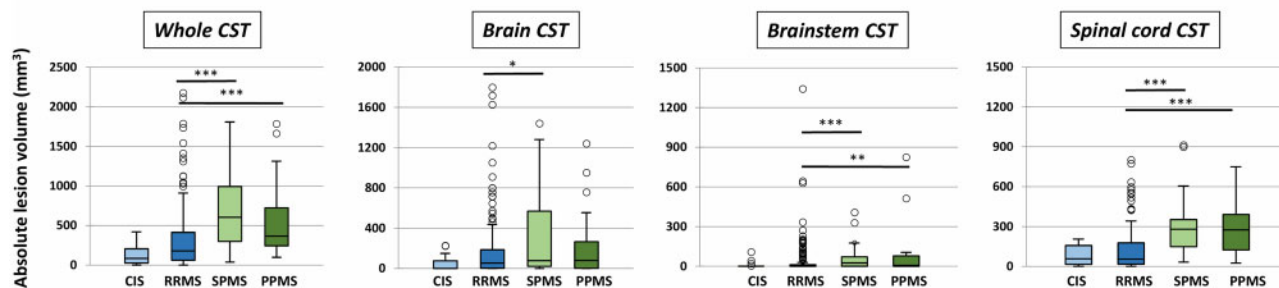
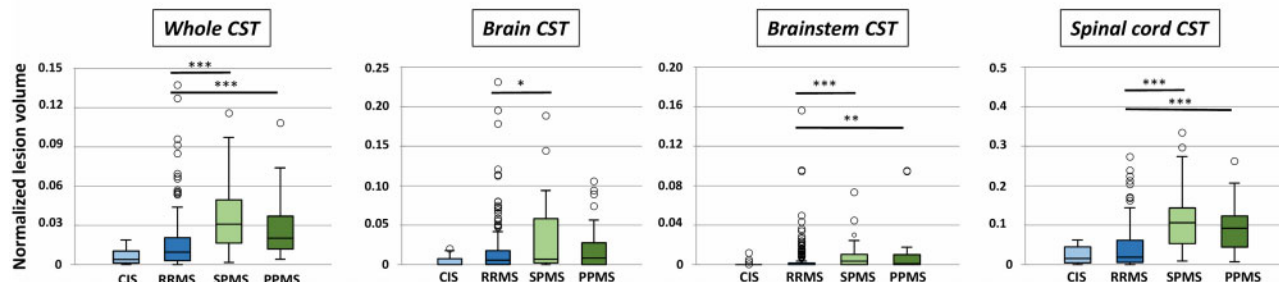
A Absolute lesion volume**B Normalized lesion volume**

Figure 4 Absolute and normalized lesion volumes for each phenotype, measured in the whole CST, in the brain, brainstem and spinal cord portion of the CST. *** $P < 0.0001$, ** $P < 0.001$, * $P < 0.05$. For clarity, only significant differences between relapsing-remitting and progressive phenotypes are reported, and not between clinically isolated syndrome and other phenotypes. For each box plot, the median is indicated as a thick horizontal line and the interquartile range as a rectangle. The horizontal bar at both extremities of the whiskers indicates the 5th and 95th percentiles. The circles indicate outliers.

functional system score (Fig. 6B), was associated with lesion frequency in the spinal cord and to a lesser extent in the brain. The strongest correlations assessed by the t -value were found in the right lateral CST at C4 for the spinal cord (peak t -value: 7.2, $P = 0.0002$) and in left corona radiata, outside the CST (in the parietal lobe), for the brain (peak t -value: 5.8, $P = 0.0006$). The voxelwise analyses were repeated without adjustment for scanning sites. The results were unchanged.

Relation between CST lesion load and location and disability at baseline

Results of the univariate correlations between MRI characteristics and EDSS, pyramidal functional system score, 9HPT and TWT score at baseline are detailed in Supplementary Table 4. Overall, the spinal cord lesion volume and the brain and spinal cord atrophy measurements demonstrated the highest correlations with disability scores. Results of multivariable models combining centre, clinical variables (age, sex, disease duration) and MRI variables (brain, brainstem, and cervical spinal cord CST normalized lesion volume, brain parenchymal fraction and spinal cord cross sectional area) are presented in Table 2. Multiple linear regression with EDSS as a dependent variable demonstrated significant associations, ordered by importance, with cervical spinal cord CST normalized lesion volume, age, disease duration, spinal cord cross sectional area, brain CST normalized lesion

volume, and brainstem CST normalized lesion volume ($R^2 = 0.60$; Table 2). By using pyramidal functional system score as the dependent variable, we found significant associations with cervical spinal cord CST normalized lesion volume, age, brain parenchymal fraction and disease duration, with an R^2 of 0.55 for the final model (Table 2). Multiple linear regression with 9HPT as a dependent variable demonstrated significant associations with age, spinal cord and brainstem CST normalized lesion volume, with an R^2 of 0.36 (Table 2). Multiple linear regression with TWT as the dependent variable demonstrated significant associations only with disease duration with an R^2 of 0.11 (Table 2).

Both lesion volume in the whole cervical spinal cord and in the cervical spinal cord CST were not included in the same model since they highly intercorrelated ($r = 0.94$, $P < 0.0001$). We observed the same collinearity with the brain measurements ($r = 0.83$, $P < 0.0001$). Results of the multiple linear models when using lesion volumes in the entire structure were very similar to that restricted to the CST (Supplementary Table 5).

Predictive relationship between baseline CST pathology and disability progression at 2 years

The multivariable logistic regression model revealed that the baseline CST spinal cord lesion volume was the only

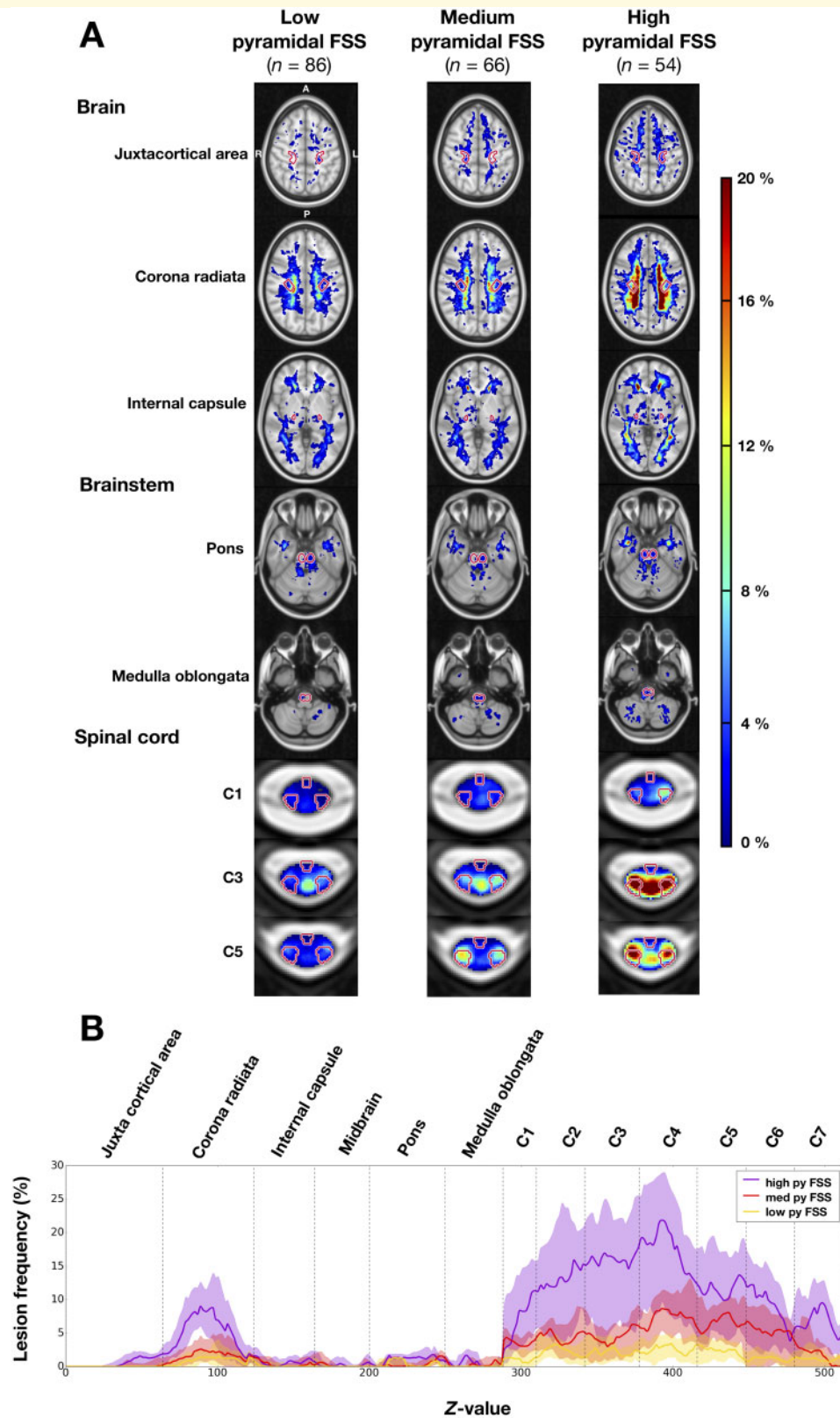


Figure 5 Frequency of multiple sclerosis lesions in the brain, brainstem and spinal cord for patients grouped by pyramidal functional system score. **(A)** Lesion frequency maps. Pyramidal functional system score (FSS) subgroups: low pyramidal functional system score (0), medium pyramidal functional system score (1–2), high pyramidal functional system score (≥ 3). The CST is indicated in red contour. **(B)** Lesion frequency along the CST for each pyramidal functional system score subcohort. For each axial slice (1-mm slice thickness), the CST lesion frequency median and interquartile range are represented by a solid line and shaded region, respectively. The CST segments are demarcated by dashed vertical lines. Pyramidal functional system score (py FSS) subgroups: low pyramidal functional system score (0), medium pyramidal functional system score (1–2), high pyramidal functional system score (≥ 3). When interpreting this graph, it is important to note that the lesion frequencies are normalized by the CST volume.

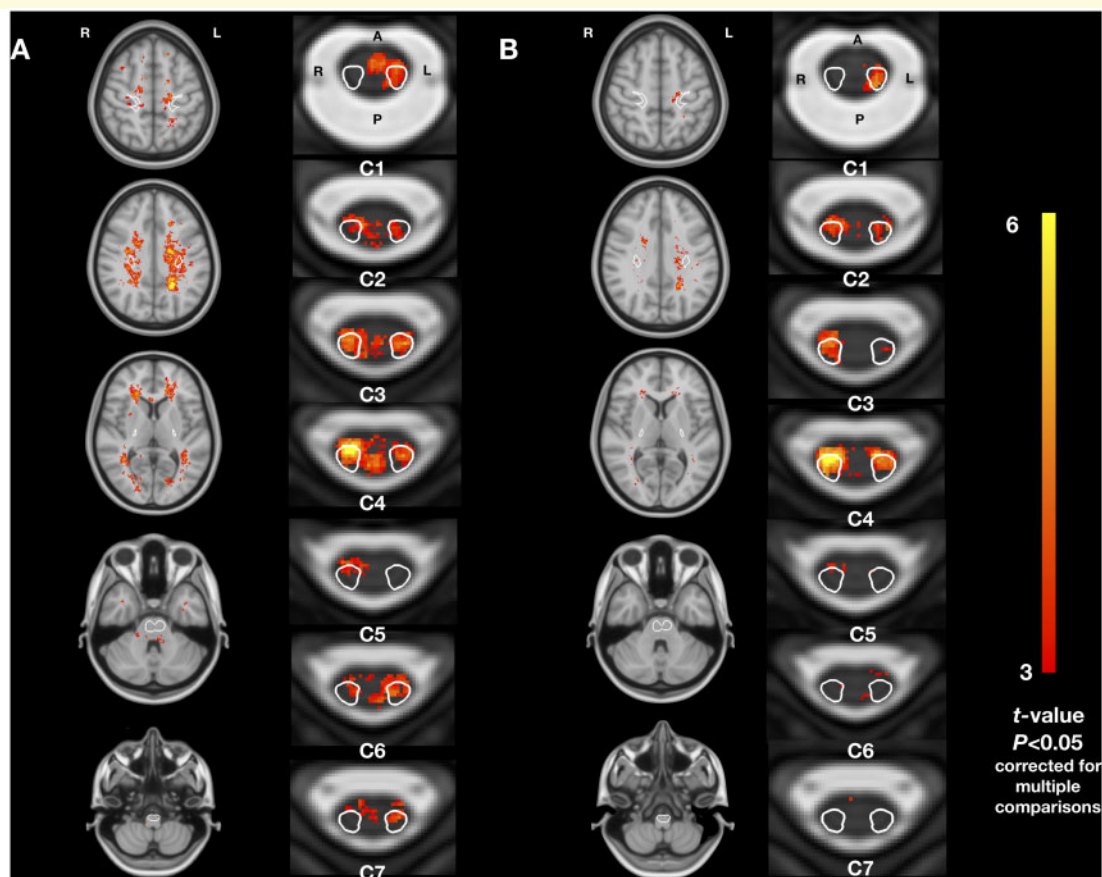


Figure 6 Association between T₂ lesion frequency and disability. (A) Disability scored by the EDSS. (B) Disability scored by the pyramidal functional system score. Only *t*-values for significant clusters are shown ($P < 0.05$, family-wise error corrected for multiple comparisons). All analyses were adjusted for sex, age, disease duration and scanning sites at a voxel scale. The CST is indicated in white contour in the axial views.

explanatory variable associated with an increased risk of EDSS progression at 2 years [OR (95%CI): 1.09 (1.03–1.17), $P = 0.003$ for the spinal cord CST normalized lesion volume expressed in percentage]. The area under the curve of the global model was 0.74. No explanatory variable was associated with an increased risk of pyramidal functional system score progression at 2 years. In the subgroup of progressive multiple sclerosis patients (46 of 70 progressive multiple sclerosis patients with available EDSS evaluation at 2 years), no explanatory variable was associated with an increased risk of EDSS progression at 2 years. Results when using normalized lesion volume in the entire cervical spinal cord were similar to those obtained when restricting to the cervical spinal cord CST.

Discussion

While previous investigations were restricted either to the brain (Riahi *et al.*, 1998; Wilson *et al.*, 2003; Reich *et al.*, 2008; Daams *et al.*, 2015; Tovar-Moll *et al.*, 2015; Fritz *et al.*, 2017) or spinal cord (Zackowski *et al.*, 2009; Naismith *et al.*, 2013; Eden *et al.*, 2019), we explored the CST lesion load from the

brain to the cervical cord since motor deficits are likely to be caused by cumulative damage along the tracts. We described the lesion distribution along the CST depending on the phenotype and disability using lesion frequency maps and further assessed these relationships using voxelwise statistical analyses. We then compared the spatial difference of lesion load by measuring the absolute and normalized lesion volume in the brain, brainstem and cervical spinal cord CST. We investigated their relative relationship with clinical measures assessing motor or ambulatory function at baseline and 2 years.

Spatial distribution of multiple sclerosis lesions along the CST

Focal lesions were not homogeneously distributed along the CST, with clear predominance in the cervical spinal cord and the corona radiata. This observation was consistent across all phenotypes. Regarding lesions in the brain, we found a higher lesion frequency adjacent to the frontal and occipital horns of lateral ventricles and in the corona radiata, which is in line with observations previously reported in other MRI (Di Perri *et al.*, 2008; Holland *et al.*, 2012) and histopathological (Haider *et al.*, 2016) studies. Interestingly,

Table 2 Multivariate linear regression of EDSS, pyramidal functional system score, 9HPT and TWT

	Standardized β coefficient ^a	SE	P-value
EDSS score ($R^2 = 0.60$)			
Age, years	0.28	0.06	<0.0001
Disease duration, years	0.18	0.07	0.007
Normalized brain CST lesion volume	0.11	0.05	0.02
Normalized brainstem CST lesion volume	0.09	0.04	0.02
Normalized cervical cord CST lesion volume	0.31	0.04	<0.0001
Spinal cord cross sectional area, mm ²	-0.12	0.06	0.02
Centre ^b			
Centre 2	-0.15	0.20	0.5
Centre 3	-0.09	0.29	0.7
Centre 5	-0.11	0.22	0.6
Centre 6	0.53	0.28	0.05
Centre 7	0.37	0.21	0.07
Centre 8	-0.09	0.22	0.7
Pyramidal functional system score ($R^2 = 0.55$)			
Age, years	0.25	0.06	<0.0001
Disease duration, years	0.16	0.07	0.02
Normalized spinal cord CST lesion volume	0.32	0.05	<0.0001
Brain parenchymal fraction	-0.20	0.06	0.0009
9HPT ($R^2 = 0.36$)			
Age, years	0.43	0.09	<0.0001
Normalized brainstem CST lesion volume	0.23	0.09	0.01
Normalized spinal cord CST lesion volume	0.28	0.07	0.0002
TWT ($R^2 = 0.11$)			
Disease duration, years	0.22	0.04	<0.0001

^aExcept for the centre.

^bPatients from Centre 4 were not included in multiple linear regression model (no disease duration available for these patients).

the M1-CST atlas fairly overlapped with high lesion frequency locations in the corona radiata, in particular in the medial part of the CST. Although this finding will require further investigation, it could have functional consequences since the CST in the corona radiata are known to be somatotopically organized (i.e. the lower limbs, the upper limbs and the face in the medial-to-lateral direction) (Duvernoy, 1999). In the spinal cord, high lesion frequency was found in the lateral and posterior funiculi, as previously described in both MRI (Kearney *et al.*, 2013; Eden *et al.*, 2019) and histopathological (Fog, 1950; Oppenheimer, 1978; Nijeholt *et al.*, 2001) studies. Unlike the brain CST, which were generally only partially affected by lesions, high lesion frequency (i.e. > 10%) was spread over a very large portion of the spinal cord CST area. Consequently, the normalized lesion volume was higher in the spinal cord CST compared to the brain CST. These results confirm those reported in early RRMS patients (Chouteau *et al.*, 2019). A previous pathological study also quantified demyelination at different levels of the CST, showing higher lesion load in the spinal cord compared to the brain (DeLuca *et al.*, 2006). In addition, an association between CST lesion and axonal loss was recently reported after excluding lesion pathology in the CST above or below the lesion of interest (Petrova *et al.*, 2018), suggesting that focal demyelination could have a significant impact on tract-specific axonal damage.

Although no clear pathological mechanism has yet been confirmed to explain this higher lesion frequency in both the corona radiata and cervical cord, MRI and pathological studies suggest an association between brain lesion location and veins (i.e. high venous density) (Tallantyre *et al.*, 2008; Haider *et al.*, 2016) and arterial anatomy (i.e. regions of low arterial blood supply) (Brownell and Hughes, 1962; Holland *et al.*, 2012; Haider *et al.*, 2016). As a consequence, a promising investigation avenue would be to precisely correlate spinal cord lesion location with arterial and venous supply.

Association between CST lesion load and location, and disease phenotypes

We observed higher lesion volume in both PPMS and SPMS compared to relapsing phenotypes in the spinal cord and the brainstem CST, and higher lesion volume in SPMS compared to relapsing phenotypes in the brain CST. Comparison of these findings is hindered by the lack of pathological or MRI studies describing lesion distribution in the whole CST according to disease phenotypes. However, when only considering the cervical section, our results are in line with recent studies quantifying the lesion load for each phenotype on 3D images (Kearney *et al.*, 2015) or on

T₁-weighted MRI (Valsasina *et al.*, 2018). In earlier studies where spinal cord lesion load was assessed with the number of lesions and involved segments, similar findings were established when comparing SPMS to RRMS (Lycklama à Nijeholt *et al.*, 1997; Filippi *et al.*, 2000; Lukas *et al.*, 2013).

It is noteworthy that progressive patients included in our study were significantly older and with a longer disease duration than RRMS patients, which could also partially explain the differences observed in lesion frequency maps between phenotypes. To mitigate this effect, our voxelwise comparisons included both age and disease duration as covariates. Results confirmed that lesion frequency was significantly higher in SPMS and PPMS patients compared to RRMS patients in specific locations such as spinal cord CST. These findings support an association between lesions location in the spinal cord CST and progressive phenotypes. Other clusters were also found outside the CST, in particular in the central and posterior spinal cord of PPMS patients. Although spinal cord grey matter lesions were more frequent than white matter lesions in pathological studies (Gilmore *et al.*, 2009; Petrova *et al.*, 2018) and were associated with disability in MRI studies (Agosta *et al.*, 2007; Kearney *et al.*, 2016), it is important to note that they were not precisely evaluated in our cohort. The majority of patients had axial T₂* acquisition, where grey matter and multiple sclerosis lesion share similar signal intensity. However, both upper and lower motor neurons are partly located in the spinal cord grey matter. Thus, spinal cord grey matter lesions could have a significant impact on motor function, in addition to CST lesions. Other significant clusters were also found in the frontal lobes of SPMS patients compared to RRMS patients, outside the CST. In our study, only the CST descending from the primary motor cortex (M1-CST) were considered. However, the CST also originate in areas beyond M1 in the premotor areas and parietal lobe (Archer *et al.*, 2018). Hence, these clusters could also have an impact on motor function.

Association between CST lesions and disability

Our results suggest that both CST lesion load and lesion location have an impact on motor disability. Thus, spinal cord CST lesion volume and, to a lesser extent, brainstem and brain CST lesion volume were independently associated with baseline EDSS. In patients with confirmed multiple sclerosis, the association between spinal cord lesion and disability had long been considered as low or moderate when spinal cord lesion load was quantified using lesion number in the sagittal plane (Lycklama à Nijeholt *et al.*, 1997; Lukas *et al.*, 2013). In contrast, recent studies showed higher association between EDSS and lesion area or volume, quantified using both sagittal and axial acquisition (Pravatà *et al.*, 2019) or 3D phase-sensitive inversion-recovery sequence (Kearney *et al.*, 2015). Similar to previous studies, we showed that

cord atrophy and patient age were independently associated with disability (Lukas *et al.*, 2013; Kearney *et al.*, 2015; Daams *et al.*, 2015), as well as brain (Lukas *et al.*, 2013; Kearney *et al.*, 2015; Daams *et al.*, 2015; Pravatà *et al.*, 2019) and brainstem lesions (Lukas *et al.*, 2013; Kearney *et al.*, 2015; Daams *et al.*, 2015). The spinal cord CST lesion volume was also the only explanatory variable associated with an increased risk of disability progression at 2 years, which is in line with previous studies highlighting the high prognostic value of spinal cord focal lesions on disability at every stage of multiple sclerosis (Sombekke *et al.*, 2013; D'Amico *et al.*, 2016; Kantarci *et al.*, 2016; Brownlee *et al.*, 2017; Arrambide *et al.*, 2018; Brownlee *et al.*, 2019). In the subgroup of progressive multiple sclerosis patients, no explanatory variable was associated with an increased risk of EDSS progression at 2 years. However, this result should be interpreted with caution because of the limited number of patients included in this analysis ($n = 46$).

Overall, our study confirmed the predominant impact of cervical lesions on motor disability, while the importance of lesions specifically located within the CST remains more difficult to establish. Thus, the multivariate linear regression of the EDSS provided similar results when the lesion volumes were measured within or not within the CST, due to collinearity between these measurements. However, voxelwise analyses showed that the most significant clusters associated with the EDSS and the pyramidal functional system score were within the spinal cord CST. Other studies including patients with progressive motor deficits while having a limited number of CNS lesions also provided arguments in favour of a relationship between lesion location within the spinal cord or brainstem CST and motor disability (Keegan *et al.*, 2016, 2018; Sechi *et al.*, 2019). Similarly, magnetization transfer imaging metrics in the spinal cord lateral column were found to correlate with motor tests such as ankle flexion strength (Zackowski *et al.*, 2009).

Finally, voxelwise analyses showed left-right asymmetric results in our study. The strongest correlations between the EDSS score and lesion frequency were found in the right lateral CST for the spinal cord and in the left corona radiata for the brain. Although we do not know the dominant side of each patient, this observation, at the population level, possibly reflects a greater impact of dominant motor pathway lesions on overall physical disability assessed by the EDSS. This observation will require confirmation but has already been reported in brain studies (Dalton *et al.*, 2012; Filli *et al.*, 2012).

Limitations and future directions

Several limitations of this study need to be discussed. First, technical drawbacks could influence the results on lesion distribution along the CST. Lesions located in the lateral part of the spinal cord are often missed on sagittal scans (Breckwoldt *et al.*, 2017) and the combination of axial and sagittal acquisition improves lesion detection, compared to sagittal scans alone (Weier *et al.*, 2012; Galler *et al.*, 2016; Breckwoldt *et al.*, 2017). Thus, unlike our previous study

(Eden *et al.*, 2019), only patients with both sagittal and axial data covering the entire cervical cord were included. Lesion volumes were computed based on axial data (instead of a weighted combination of both sagittal and axial data), leading to a higher lesion frequency in the CST than previously reported. We also observed a lower image quality in the lower part of the cervical spinal cord, which could partially explain the lower lesion frequency reported at these levels due to acquisition limitations. Indeed, the lesion load difference between the upper and lower cervical cord is in divergence with pathological studies (DeLuca *et al.*, 2006; Petrova *et al.*, 2018). CST lesions were also possibly underestimated in the brainstem, where artefacts are frequent. In our study, 3D T₂-FLAIR and axial T₂ images were available in a large majority of patients and both were used to help lesion identification.

Second, our evaluation of the CST excluded the thoracic and lumbar portions due to the lack of data in this area, which is still challenging to image. Recent studies described the distribution of multiple sclerosis lesions in the thoracic section (Weier *et al.*, 2012; Galler *et al.*, 2016; Pravatà *et al.*, 2019), and further studies are now needed to evaluate the added value of thoracic CST lesions to explain motor disability in multiple sclerosis patients.

Third, the CST delineation is sensitive to errors of registration, especially because of the small size of these tracts. To mitigate registration inaccuracies, a multistep registration process, including non-linear transformations, has been tailored for this dataset and all cases have been visually inspected. For the brain CST identification, probabilistic tractography (Chouteau *et al.*, 2019) or atlas-based analyses of diffusion data (Bazin *et al.*, 2011) would have been alternative options. An atlas-based method on 3D T₁-weighted images was preferred in this multicentre large-scale study due to the lack of diffusion acquisitions in some centres and the variability of diffusion protocols used. To validate this method, we compared the results of the atlas- and tractography-based methods in a subset of patients. The results were highly correlated. In addition, a joint CST atlas between the brain and brainstem area would be of great interest, since the atlases used in this study overlap on a few slices where the voxel-wise weights differ. To overcome this issue, both templates have been cropped and further connected ($z = 63$ in the MNI space) so that the joint atlas distribution was consistent along the inferior-to-superior direction.

Fourth, the clinical evaluation of motor function was limited to the EDSS, pyramidal functional system score, TWT and 9HPT. These tests do not provide unilateral and precise evaluation of the motor function which is likely to hinder the correlation between CST lesion load and motor disability. As motor deficits are often asymmetric in multiple sclerosis patients, it could be of great interest to correlate the right and the left motor function with the associated motor tract lesion load.

Limitations in the assessment of disability progression must also be raised. Indeed, 2 years follow-up is a short period of time to identify disability worsening, and disability

progression was defined as an increase in the EDSS of at least 1 point if the baseline EDSS was ≤ 5.5 , or 0.5 point if > 5.5 , without any additional restrictive criteria (i.e. confirmed disability progression at 6 months).

In addition, the T₂ hyperintensities visible on MRI and traditionally considered as multiple sclerosis lesions lack of specificity for demyelination (Trapp *et al.*, 2018). This key element probably explains the only moderate correlation found between CST lesion load and motor impairment.

Finally, an important limitation of this study is the lack of evaluation of diffuse damage along the CST, outside the lesions. Future work could explore the benefit of including diffusion and/or magnetization transfer-derived metrics along the CST in order to clarify the contribution of demyelination in CST focal lesion to remote Wallerian degeneration in the same tract. This key question would also benefit from longitudinal studies. In particular, the prognostic impact of early CST focal lesions, related to the inflammatory demyelinating process, on long term disability progression, probably related to axonal and neuronal death, is a critical issue and would have strong practical implication (Mahad *et al.*, 2015). The long-term goal would be to provide the clinician with a biomarker able to plan therapeutic decisions and support the switch to more aggressive treatment or intensive rehabilitation program in order to maintain motor function.

Conclusion

In this study, we assessed CST lesion load from the cerebral cortex to the cervical spinal cord in a large population of multiple sclerosis patients. We used brain and spinal cord MRI conventional sequences, processed by an automatic and publicly available pipeline. We demonstrated that multiple sclerosis lesions are not homogeneously distributed along the CST, with predominant locations in the cervical spinal cord and the corona radiata. The spinal cord, brainstem and brain CST lesion load are higher in progressive compared to relapsing multiple sclerosis patients and are associated with disability, independently from spinal cord atrophy. Finally, spinal cord CST lesions at baseline are associated with an increased risk of disability progression at 2 years. Overall, our results suggest a cumulative effect of lesions within the corticospinal tracts to explain physical disability in multiple sclerosis patients, with a predominant impact of intramedullary lesions. These observations help to understand the anatomic substrate of motor impairment in multiple sclerosis patients.

Acknowledgements

The authors thank Dominique Eden for opening the door to the present study, Benjamin De Leener for the fruitful discussions and Aurélien Gilliot for his help to correct brain lesion masks.

Funding

A.K. received scholarships from ARSEP and CHU de Rennes for this research. C.G. received a scholarship from IVADO [EX-2018-4]. A.B. was supported by a Doctoral TransMedTech excellence scholarship. MRI and clinical data acquisition from Rennes, Montpellier and Marseille were supported by the French Hospital Program of Clinical Research (PHRC). This study was partially supported by the Intramural Research Program of the National Institute of Neurological Disorders and Stroke, National Institutes of Health (USA). This MS research was funded by the Swedish Research Council and the Swedish Brain Foundation.

Competing interests

A.K., C.G., A.B., E.B., F.G., B.C., R.C., P.L., X.A., C.C.D., J.M., T.G., R.O., L.S., J.T., Y.T., M.K., K.K., L.C., J.L., D.S.R., G.N., P.V., R.C., V.C., J.P., B.A., A.M., N.C., J.D., G.E., J.C.-A. report no potential conflicts of interest with respect to this research. M.A.R. received speaker's honoraria from Biogen Idec, Novartis, Genzyme, Teva, Merck Serono, Roche, Celgene and Bayer and receives research support from the Italian Ministry of Health, MS Society of Canada and Fondazione Italiana Sclerosi Multipla. M.F. is Editor-in-Chief of the *Journal of Neurology*; received compensation for consulting services and/or speaking activities from Biogen Idec, Merck-Serono, Novartis, Sanofi Genzyme, Takeda, Teva Pharmaceutical Industries; and receives research support from Biogen Idec, Merck-Serono, Novartis, Teva Pharmaceutical Industries, Roche, Italian Ministry of Health, Fondazione Italiana Sclerosi Multipla, and ARiSLA (Fondazione Italiana di Ricerca per la SLA). R.B. has received consulting fees from Bayer, Biogen, Celgene, EMD Serono, Genentech, Guerbet, Novartis, Sanofi-Genzyme, and Shire and research support from EMD Serono and Sanofi-Genzyme. J.H. has received honoraria for serving on advisory boards for Biogen, Sanofi-Genzyme and Novartis and speaker's fees from Biogen, Novartis, Merck-Serono, Bayer-Schering, Teva and Sanofi-Genzyme. He has served as P.I. for projects or received unrestricted research support from, Biogen Idec, Merck, Novartis and Sanofi-Genzyme.

Supplementary material

Supplementary material is available at *Brain* online.

References

Agosta F, Pagani E, Caputo D, Filippi M. Associations between cervical cord gray matter damage and disability in patients with multiple sclerosis. *Arch Neurol* 2007; 64: 1302–5.
 Archer DB, Vaillancourt DE, Coombes SA. A Template and Probabilistic Atlas of the Human Sensorimotor Tracts using Diffusion MRI. *Cereb Cortex* 2018; 28: 1685–99.

Arrambide G, Rovira A, Sastre-Garriga J, Tur C, Castelló J, Río J, et al. Spinal cord lesions: a modest contributor to diagnosis in clinically isolated syndromes but a relevant prognostic factor. *Mult Scler* 2018; 24: 301–12.
 Avants BB, Tustison NJ, Wu J, Cook PA, Gee JC. An open source multivariate framework for n-tissue segmentation with evaluation on public data. *Neuroinform* 2011; 9: 381–400.
 Barkhof F. The clinico-radiological paradox in multiple sclerosis revisited. *Curr Opin Neurol* 2002; 15: 239–45.
 Bazin P-L, Ye C, Bogovic JA, Shiee N, Reich DS, Prince JL, et al. Direct segmentation of the major white matter tracts in diffusion tensor images. *Neuroimage* 2011; 58: 458–68.
 Breckwoldt MO, Gradl J, Hähnel S, Hielscher T, Wildemann B, Diem R, et al. Increasing the sensitivity of MRI for the detection of multiple sclerosis lesions by long axial coverage of the spinal cord: a prospective study in 119 patients. *J Neurol* 2017; 264: 341–9.
 Brownell B, Hughes JT. The distribution of plaques in the cerebrum in multiple sclerosis. *J Neurol Neurosurg Psychiatry* 1962; 25: 315–20.
 Brownlee WJ, Altmann DR, Alves Da Mota P, Swanton JK, Miszkial KA, Wheeler-Kingshott CG, et al. Association of asymptomatic spinal cord lesions and atrophy with disability 5 years after a clinically isolated syndrome. *Mult Scler* 2017; 23: 665–74.
 Brownlee WJ, Altmann DR, Prados F, Miszkial KA, Eshaghi A, Gandini Wheeler-Kingshott CG, et al. Early imaging predictors of long-term outcomes in relapse-onset multiple sclerosis. *Brain* 2019; 142: 2276–87.
 Chouteau R, Combès B, Bannier E, Snoussi H, Ferré J-C, Barillot C, et al. Joint assessment of brain and spinal cord motor tract damage in patients with early RRMS: predominant impact of spinal cord lesions on motor function. *J Neurol* 2019; 266: 2294–303.
 Commowick O, Wiest-Daessle N, Prima S. Block-matching strategies for rigid registration of multimodal medical images. In: 2012 9th IEEE International Symposium on Biomedical Imaging (ISBI). 2012. Available from: <http://dx.doi.org/10.1109/isbi.2012.6235644>.
 Daams M, Steenwijk MD, Wattjes MP, Geurts JJG, Uitdehaag BMJ, Tevarie PK, et al. Unraveling the neuroimaging predictors for motor dysfunction in long-standing multiple sclerosis. *Neurology* 2015; 85: 248–55.
 Dalton C, Bodini B, Samson R, Battaglini M, Fisniku L, Thompson A, et al. Brain lesion location and clinical status 20 years after a diagnosis of clinically isolated syndrome suggestive of multiple sclerosis. *Mult Scler* 2012; 18: 322–8.
 D'Amico E, Patti F, Leone C, Lo Fermo S, Zappia M. Negative prognostic impact of MRI spinal lesions in the early stages of relapsing–remitting multiple sclerosis. *Multiple Sclerosis Journal–Experimental, Translational and Clinical* 2016; 2: 2055217316631565.
 De Leener B, Fonov VS, Collins DL, Callot V, Stikov N, Cohen-Adad J. PAM50: unbiased multimodal template of the brainstem and spinal cord aligned with the ICBM152 space. *Neuroimage* 2018; 165: 170–9.
 De Leener B, Lévy S, Dupont SM, Fonov VS, Stikov N, Louis Collins D, et al. SCT: spinal Cord Toolbox, an open-source software for processing spinal cord MRI data. *Neuroimage* 2017; 145: 24–43.
 DeLuca GC, Williams K, Evangelou N, Ebers GC, Esiri MM. The contribution of demyelination to axonal loss in multiple sclerosis. *Brain* 2006; 129: 1507–16.
 Di Perri C, Battaglini M, Stromillo ML, Bartolozzi ML, Guidi L, Federico A, et al. Voxel-based assessment of differences in damage and distribution of white matter lesions between patients with primary progressive and relapsing–remitting multiple sclerosis. *Arch Neurol* 2008; 65: 236–43.
 Duvernoy HM. The human brain: surface, blood supply, and three-dimensional anatomy. Wien NY: Springer Verlag; 1999.
 Eden D, Gros C, Badji A, Dupont SM, De Leener B, Maranzano J, et al. Spatial distribution of multiple sclerosis lesions in the cervical spinal cord. *Brain* 2019; 142: 633–46.
 Filippi M, Bozzali M, Horsfield MA, Rocca MA, Sormani MP, Iannucci G, et al. A conventional and magnetization transfer MRI study of the cervical cord in patients with MS. *Neurology* 2000; 54: 207.

- Filli L, Hofstetter L, Kuster P, Traud S, Mueller-Lenke N, Naegelin Y, et al. Spatiotemporal distribution of white matter lesions in relapsing–remitting and secondary progressive multiple sclerosis. *Mult Scler* 2012; 18: 1577–84.
- Fischer JS, Rudick RA, Cutter GR, Reingold SC. The Multiple Sclerosis Functional Composite: an integrated approach to MS clinical outcome assessment. *Mult Scler* 1999; 5: 244–50.
- Fog T. Topographic distribution of plaques in the spinal cord in multiple sclerosis. *Arch Neuropsych* 1950; 63: 382–414.
- Fritz NE, Keller J, Calabresi PA, Zackowski KM. Quantitative measures of walking and strength provide insight into brain corticospinal tract pathology in multiple sclerosis. *Neuroimage Clin* 2017; 14: 490–8.
- Galler S, Stellmann J-P, Young KL, Kutzner D, Heesen C, Fiehler J, et al. Improved lesion detection by using axial T2-Weighted MRI with full spinal cord coverage in multiple sclerosis. *AJNR Am J Neuroradiol* 2016; 37: 963–9.
- Gilmore CP, Geurts JJG, Evangelou N, Bot JCJ, van Schijndel RA, Pouwels PJW, et al. Spinal cord grey matter lesions in multiple sclerosis detected by post-mortem high field MR imaging. *Mult Scler* 2009; 15: 180–8.
- Gros C, De Leener B, Badji A, Maranzano J, Eden D, Dupont SM, et al. Automatic segmentation of the spinal cord and intramedullary multiple sclerosis lesions with convolutional neural networks. *NeuroImage* 2019; 184: 901–15.
- Haider L, Zrzavy T, Hametner S, Höftberger R, Bagnato F, Grabner G, et al. The topography of demyelination and neurodegeneration in the multiple sclerosis brain. *Brain* 2016; 139: 807–15.
- Healy BC, Buckle GJ, Ali EN, Egorova S, Khalid F, Tauhid S, et al. Characterizing clinical and MRI dissociation in patients with multiple sclerosis. *J Neuroimaging* 2017; 27: 481–5.
- Holland CM, Charil A, Csapo I, Liptak Z, Ichise M, Khoury SJ, et al. The relationship between normal cerebral perfusion patterns and white matter lesion distribution in 1,249 patients with multiple sclerosis. *J Neuroimaging* 2012; 22: 129–36.
- Kantarci OH, Lebrun C, Siva A, Keegan MB, Azevedo CJ, Inglese M, et al. Primary progressive multiple sclerosis evolving from radiologically isolated syndrome. *Ann Neurol* 2016; 79: 288–94.
- Kearney H, Altmann DR, Samson RS, Yiannakas MC, Wheeler-Kingshott C, Ciccarelli O, et al. Cervical cord lesion load is associated with disability independently from atrophy in MS. *Neurology* 2015; 84: 367–73.
- Kearney H, Miszkil KA, Yiannakas MC, Altmann DR, Ciccarelli O, Miller DH. Grey matter involvement by focal cervical spinal cord lesions is associated with progressive multiple sclerosis. *Mult Scler* 2016; 22: 910–20.
- Kearney H, Miszkil KA, Yiannakas MC, Ciccarelli O, Miller DH. A pilot MRI study of white and grey matter involvement by multiple sclerosis spinal cord lesions. *Mult Scler Relat Disord* 2013; 2: 103–8.
- Keegan BM, Kaufmann TJ, Weinschenker BG, Kantarci OH, Schmalstieg WF, Paz Soldan MM, et al. Progressive solitary sclerosis: gradual motor impairment from a single CNS demyelinating lesion. *Neurology* 2016; 87: 1713–9.
- Keegan BM, Mark Keegan B, Kaufmann TJ, Weinschenker BG, Kantarci OH, Schmalstieg WF, et al. Progressive motor impairment from a critically located lesion in highly restricted CNS-demyelinating disease. *Mult Scler* 2018; 24: 1445–52.
- Kurtzke JF. Rating neurologic impairment in multiple sclerosis: an expanded disability status scale (EDSS). *Neurology* 1983; 33: 1444–52.
- Lattanzi S, Logullo F, Di Bella P, Silvestrini M, Provinciali L. Multiple sclerosis, solitary sclerosis or something else?. *Mult Scler* 2014; 20: 1819–24.
- Lévy S, Benhamou M, Naaman C, Rainville P, Callot V, Cohen-Adad J. White matter atlas of the human spinal cord with estimation of partial volume effect. *Neuroimage* 2015; 119: 262–71.
- Lublin FD, Reingold SC, Cohen JA, Cutter GR, Sørensen PS, Thompson AJ, et al. Defining the clinical course of multiple sclerosis: the 2013 revisions. *Neurology* 2014; 83: 278–86.
- Lukas C, Sombekke MH, Bellenberg B, Hahn HK, Popescu V, Bendfeldt K, et al. Relevance of spinal cord abnormalities to clinical disability in multiple sclerosis: MR imaging findings in a large cohort of patients. *Radiology* 2013; 269: 542–52.
- Lycklama À Nijeholt GJ, Barkhof F, Scheltens P, Castelijns JA, Adèr H, van Waesberghe JH, et al. MR of the spinal cord in multiple sclerosis: relation to clinical subtype and disability. *AJNR Am J Neuroradiol* 1997; 18: 1041–8.
- Mahad DH, Trapp BD, Lassmann H. Pathological mechanisms in progressive multiple sclerosis.[review]. *Lancet Neurol* 2015; 14: 183–93.
- Naismith RT, Xu J, Klawiter EC, Lancia S, Tutlam NT, Wagner JM, et al. Spinal cord tract diffusion tensor imaging reveals disability substrate in demyelinating disease. *Neurology* 2013; 80: 2201–9.
- Nijeholt G. À, Bergers E, Kamphorst W, Bot J, Nicolay K, Castelijns JA, et al. Post-mortem high-resolution MRI of the spinal cord in multiple sclerosis. A correlative study with conventional MRI, histopathology and clinical phenotype. *Brain* 2001; 124: 154–66.
- Oppenheimer DR. The cervical cord in multiple sclerosis. *Neuropathol Appl Neurobiol* 1978; 4: 151–62.
- Petrova N, Carassiti D, Altmann DR, Baker D, Schmierer K. Axonal loss in the multiple sclerosis spinal cord revisited. *Brain Pathol* 2018; 28: 334–48.
- Pravatà E, Valsasina P, Gobbi C, Zecca C, Riccitelli GC, Filippi M, et al. Influence of CNS T2-focal lesions on cervical cord atrophy and disability in multiple sclerosis. *Mult Scler* 2019; 25: 1352458519865989.
- Reich DS, Zackowski KM, Gordon-Lipkin EM, Smith SA, Chodkowski BA, Cutter GR, et al. Corticospinal tract abnormalities are associated with weakness in multiple sclerosis. *AJNR Am J Neuroradiol* 2008; 29: 333–9.
- Riahi F, Zijdenbos A, Narayanan S, Arnold D, Francis G, Antel J, et al. Improved correlation between scores on the expanded disability status scale and cerebral lesion load in relapsing-remitting multiple sclerosis. Results of the application of new imaging methods. *Brain* 1998; 121: 1305–12.
- Sechi E, Keegan BM, Kaufmann TJ, Kantarci OH, Weinschenker BG, Flanagan EP. Unilateral motor progression in MS: association with a critical corticospinal tract lesion. *Neurology* 2019; 93: e628–e634.
- Smith SM, Nichols TE. Threshold-free cluster enhancement: addressing problems of smoothing, threshold dependence and localisation in cluster inference. *Neuroimage* 2009; 44: 83–98.
- Sombekke MH, Wattjes MP, Balk LJ, Nielsen JM, Vrenken H, Uitendhaag BMJ, et al. Spinal cord lesions in patients with clinically isolated syndrome: a powerful tool in diagnosis and prognosis. *Neurology* 2013; 80: 69–75.
- Suarez RO, Commowick O, Prabhu SP, Warfield SK. Automated delineation of white matter fiber tracts with a multiple region-of-interest approach. *Neuroimage* 2012; 59: 3690–700.
- Tallantyre EC, Brookes MJ, Dixon JE, Morgan PS, Evangelou N, Morris PG. Demonstrating the perivascular distribution of MS lesions in vivo with 7-Tesla MRI. *Neurology* 2008; 70: 2076–8.
- Tang Y, Sun W, Toga AW, Ringman JM, Shi Y. A probabilistic atlas of human brainstem pathways based on connectome imaging data. *Neuroimage* 2018; 169: 227–39.
- Thompson AJ, Banwell BL, Barkhof F, Carroll WM, Coetzee T, Comi G, et al. Diagnosis of multiple sclerosis: 2017 revisions of the McDonald criteria. *Lancet Neurol* 2018; 17: 162–73.
- Tovar-Moll F, Evangelou IE, Chiu AW, Auh S, Chen C, Ehrmantraut M, et al. Diffuse and focal corticospinal tract disease and its impact on patient disability in multiple sclerosis. *J Neuroimaging* 2015; 25: 200–6.
- Trapp B, Vignos M, Dudman J, Chang A, Fisher E, Staugaitis S, et al. Cortical neuronal loss and white matter demyelination in multiple sclerosis: a retrospective study. *Lancet Neurol* 2018; 17: 870–84.
- Valsasina P, Aboulwafa M, Preziosa P, Messina R, Falini A, Comi G, et al. Cervical cord T1-weighted hypointense lesions at MR imaging

- in multiple sclerosis: relationship to cord atrophy and disability. *Radiology* 2018; 288: 234–44.
- Valverde S, Cabezas M, Roura E, González-Villà S, Pareto D, Vilanova JC, et al. Improving automated multiple sclerosis lesion segmentation with a cascaded 3D convolutional neural network approach. *Neuroimage* 2017; 155: 159–68.
- Weier K, Mazraeh J, Naegelin Y, Thoeni A, Hirsch JG, Fabbro T, et al. Biplanar MRI for the assessment of the spinal cord in multiple sclerosis. *Mult Scler* 2012; 18: 1560–9.
- Wilson M, Tench CR, Morgan PS, Blumhardt LD. Pyramidal tract mapping by diffusion tensor magnetic resonance imaging in multiple sclerosis: improving correlations with disability. *J Neurol Neurosurg Psychiatry* 2003; 74: 203–7.
- Zackowski KM, Smith SA, Reich DS, Gordon-Lipkin E, Chodkowski BA, Sambandan DR, et al. Sensorimotor dysfunction in multiple sclerosis and column-specific magnetization transfer-imaging abnormalities in the spinal cord. *Brain* 2009; 132: 1200–9.